Dynamic conductivity and plasmon profile of aluminum in the ultra-fast-matter regime

M. W. C. Dharma-wardana*
National Research Council of Canada, Ottawa, Canada, K1A 0R6
(Received 23 January 2016; revised manuscript received 14 May 2016; published 14 June 2016)

We use an explicitly isochoric two-temperature theory to analyze recent x-ray laser scattering data for aluminum in the ultra-fast-matter (UFM) regime up to 6 eV. The observed surprisingly low conductivities are explained by including strong electron-ion scattering effects using the phase shifts calculated via the neutral-pseudo-atom model. The difference between the static conductivity for UFM-Al and equilibrium aluminum in the warm-dense matter state is clearly brought out by comparisons with available density-fucntional+molecular-dynamics simulations. Thus the applicability of the Mermin model to UFM is questioned. The static and dynamic conductivity, collision frequency, and the plasmon line shape, evaluated within the simplest Born approximation for UFM aluminum, are in good agreement with experiment.

DOI: 10.1103/PhysRevE.93.063205

I. INTRODUCTION

Short-pulsed x-ray photons, e.g., from the Linac Coherent Light Source (LCLS), have begun to provide data in hitherto-inaccessible regimes of matter [1,2]. Such information is of interest in understanding normal matter under extreme conditions [3–6], as well as at new frontiers in high-energy-density matter, astrophysics, fusion physics, etc. Such nonequilibrium systems are also produced in semiconductor devices [7]. The theory involves complicated quantum many-body effects of finite-temperature nonequilibrium systems. Standard *ab initio* methods are inapplicable or computationally prohibitive for this ultrafast matter (UFM) regime. Extensions of elementary plasma models or Thomas-Fermi models fail badly. Hence computationally simple realistic theories of these systems are essential in the interpretation of experiments on UFM which is a subclass of warm dense matter (WDM) [8]. Here we use a finite-T density-functional-theory (DFT) calculation of the electronic charge distribution $n(r)$ and the ion charge distribution $\rho(r)$ around an Al ion in the system as the basic ingredient of such a theory. The neutral pseudoatom (NPA) model of Perrot and Dharma-wardana [9–11] is used in this study.

The LCLS results [1] of the plasmon feature and the dynamic and static conductivities σ of Al up to 6 eV, isochorically held at solid density, dramatically improve on the accuracy of the earlier UFM experiments [6,12]. Surprisingly low static conductivities $\sigma(0)$ of UFM aluminum are reported in Ref. [1], even at 0.2 eV.

We present two-temperature ($2T$) calculations for isochoric aluminum. Atomic units (a.u., $|e| = \hbar = m_e = 1$) are used, and the temperature is in energy units. The ion temperature T_i is the initial "room" temperature, while only the electron temperature T_e is likely to be raised to 6 eV by the 50 fs x-ray pulse. Sperling *et al.* [1] have presented experimental evidence to support a $T_e = 6$ eV but no evidence for the ion temperature T_i. A two-temperature $2T$ model may be sufficient [4,6] or too simplistic, as in Medvedev *et al.* [13], pointing to nonequilibrium electron distributions, but the experimental information is insufficient to go beyond a $2T$ model. Using such a $2T$ model, we do not get the gradual decrease of $\sigma(0)$ with T found for equilibrium nonisochoric aluminum. Instead, we reproduce the low static conductivities reported in the experiment. The high conductivities of the normal solid and the molten metal ($T_e = T_i$) at low T are partly attributed to the position of the scattering momentum $2k_F$ *falling within the second minimum* in the ion-ion structure factor $S(q)$. In an isochoric UFM solid, the ions have no time to adjust to the rapidly heated electrons. The ions (and their bound electrons) remain frozen at their lattice sites, and at T_i. Hence $S(q)$, and the bare electron-ion pseudopotential $W(q)$, remain essentially unchanged, even up to $T_e = 6$ eV. The thermal smearing of the Fermi sphere is set by $f'(k,T_e) = f(k,T_e)[1 - f(k,T_e)]$, where $f(k,T_e)$ is the electron Fermi function. Its overlap with the ion-ion $S(q)$ and the electron-ion scattering cross section determine the conductivity $\sigma(0)$ as well as $\sigma(\omega)$.

The experiment provides the profile of the plasmon resonance. We present a simple theory of the momentum relaxation and energy dephasing frequency $\nu(\omega)$ (also known as the "collision frequency"), using a Born approximation constructed to match the $\omega \to 0$ conductivity obtained from the NPA phase shifts. The calculated plasmon profile is in good accord with experiment.

II. THE DFT-NPA MODEL FOR ISOCHORIC UFM ALUMINUM

Currently, several NPA models are referred to in the literature. The model used here [9,10] considers an aluminum nucleus placed in an electron subsystem and an ion subsystem, with the nucleus defining the center of a "correlation sphere" ($R \sim 30$ a.u.) large enough to ensure that all interparticle correlations reach bulk values as $r \to R$. Thus, unlike in "average-atom cell-models" [14], the interacting electron system is mapped to a noninteracting Kohn-Sham system with the noninteracting chemical potential μ^0, and at the density of the interacting system, as required by density-functional theory. This voids any ambiguities in fixing the chemical potential [15]. The bulk electron density, viz., n_e is 1.81×10^{23} electrons/cm^3 and has an electron-sphere radius $r_s = 2.07$ a.u. The free-electron pileup $n_f(r)$ and the scattering phase shifts δ_{kl} around the Al nucleus are calculated via the Kohn-Sham equations. A step function mimics the ion-ion pair distribution function $g(r)$ and works well for Al [10] for the purpose of

*chandre.dharma-wardana@nrc-cnrc.gc.ca

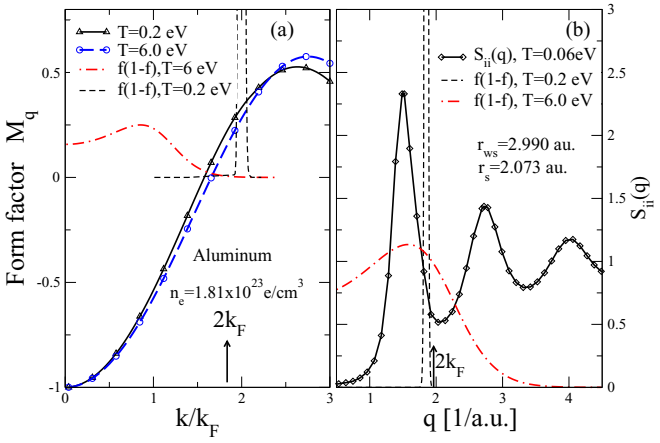

FIG. 1. (a) The pseudopotential form factor $M(q)$ at $T = 0.2$ eV and 6 eV, and the thermal-smearing functions $f'(k,T_e) = f(k)[1 - f(k)]$. (b) The overlap of $S(q)$ and $f'(k,T_e)$. The ion $S(q,T_i)$ with $T_i = 0.06$ eV.

calculating Kohn-Sham eigenstates. The phase shifts satisfy the Friedel sum rule, and the DFT formulation uses a finite-T exchange-correlation contribution [16,17]. All subsequent calculations use inputs from this DFT-NPA calculation. The many-ion system is built up as a superposition of NPAs, using the $S(q)$ derived within the theory.

At room temperature, the NPA yields an ionization $Z = 3$ and an ion Wigner-Seitz radius $r_{\rm ws} \simeq 2.99$ a.u. The $r_{\rm ws}$ is held constant while T_e is increased, to mimic the isochoric UFM, where as normal solid or liquid Al expands (i.e, $r_{\rm ws}$ increases) with temperature. A static electron response function $\chi(q,T_e)$ is constructed, with its local field correction (LFC) satisfying the compressibility sum rule at each temperature. This defines a fully local pseudopotential $W(q) = n_f(q)/\chi(q,T_e)$, and an ion-ion pair potential $U_{ii}(q) = Z^2 V_q + |W(q)|^2\chi(q)$. The pseudopotential $W(q) = -ZV_qM_q$, $V_q = 4\pi/q^2$ is fitted to a Heine-Abarenkov form for convenience. The form factor $M_q = n_f(q)/n_f^0(q)$ obtained from the NPA is shown in Fig. 1(a) at $T = 0.2$ and 6 eV. Here $n_f^0(q)$ is the linear-response charge pileup. Thus the electron-ion and ion-ion interactions are constructed entirely from Kohn-Sham quantities. This approach is capable of millivolt accuracy and reproduces even WDM phonons [18] as discussed by, e.g., Recoules *et al.* [19] (but phonons do not form during UFM time scales).

The resulting $U_{ii}(q)$ is used in the modified hyper-netted-chain equation (MHNC), yielding the $S(q)$ at the ion temperature T_i (which is the initial temperature at the arrival of the x-ray pulse). Since the initial Al-crystal has an FCC structure, we use the spherically averaged $S(q)$ taken as a "frozen fluid," say, at 0.06 eV. This is the lowest temperature at which the HNC could be converged, since the melting point is $\simeq$0.082 eV. The results are insensitive to the use of an $S(q)$ at 0.06 eV or, say, 0.082 eV. Our MHNC accurately reproduces the $S(q)$ of normal liquid aluminum [20].

III. THE COMPLEX CONDUCTIVITY $\sigma(\omega)$

The Drude theory with a static $\nu(0)$ is inadequate for $\sigma(\omega)$ except at small and high ω [21]. Sperling *et al.* [1] have used a Mermin model (diffusion pole) [22] augmented by plasma many-body theory [23]. They use a sum of Born (B), Lenard-Balescu (LB) Gould-DeWitt(GDW), and Mermin (M) approaches in their analysis where $T_i = T_e$. The real part of the complex conductivity $\sigma(\omega) = \sigma_1 + i\sigma_2$, obtained via B-LB-GDW-M, is two orders of magnitude too large compared to experiment, although the imaginary part $\sigma_2(\omega)$ and the plasmon profile are in better accord. They use several models of $S(q)$, point-ion Coulomb potentials, as well as pseudopotentials, but the $S(q)$ is not derived from the pseudopotentials used. The theory of the Mermin response assumes that the ions have sufficient time to respond to the electron-density fluctuations. This is true if time scales t are much larger than the electron-ion temperature relaxation time τ_{ei} which is many picoseconds [24] if $T_i \neq T_e$ or for time scales significantly larger than phonon time scales if $T_i = T_e$. Thus the Mermin model is largely inappropriate for most UFM-WDM systems. Furthermore, no low-ω "diffusion pole" is seen in the experimental spectra, as expected from Mermin theory.

In our approach, the ion-$S(q,T_i)$ at T_i remains intact for all T_e. We use a simple model where the ions are mere immobile scatterers during the 50-fs signal and obtain good agreement with experiment using a simple Born approximation that has been refitted to capture strong electron-ion scattering effects, as explained below.

The conductivity $\sigma(\omega) = \omega_p^2\tau(\omega)/4\pi$, where $\tau(\omega)$, i.e., $1/\nu(\omega)$ is the relaxation time and ω_p is the plasma frequency. It can can be expressed via the force-force correlation function as given in standard texts (e.g., Ref. [25], Sec. 4.6). The Born approximation formula for the relaxation frequency is

$$\nu(\omega) = \frac{1}{6\pi^2 Z}\int q^4|W(q)|^2 S(q,T_i)\Delta(q,\omega)dq, \qquad (1)$$

$$\Delta(q,\omega) = \frac{\{\chi_e(q,\omega,T_e) - \chi_e(q,0,T_e)\}}{i\omega}. \qquad (2)$$

Equation (1) is basically Hopfield's formula [21] for the dynamic relaxation frequency $\nu(\omega)$ in the Born approximation. Modern discussions are found in Refs. [23,26]. The relevant $S(q)$ in our $2T$ model is for cold ions at $T_i = 0.06$ eV, as shown in Fig. 1(b).

The limit $\omega \to 0$ gives the static relaxation frequency $\nu(0)$ and Eq. (1) reduces to the Ziman formula for the static conductivity $\sigma(0)$ which uses a weak electron-ion pseudopotential, viz., the $W(q)$ given in Fig. 1. However, it predicts a somewhat higher conductivity than reported in the LCLS experiment. Thus the electron-ion scattering is manifestly stronger than predicted from our linear-response pseudopotential or as found by Sjostrom *et al.* [27] using DFT+MD with $T_e = Ti$. The $\sigma(0)$ data from Sperling *et al.*, shown in Fig. 7 of Ref. [27], calculated for $T_e = T_i$, cannot be correct as they disagree strongly with the MD simulation [27]. Furthermore, we noted that their $S(q)$ are not calculated to be consistent with the pseudopotentials they employ. Hence we turn to the phase-shift formulation of the conductivity [28] to include strong collisions.

$$\nu(0) = \frac{1}{3\pi Z T_e}\int_0^\infty f(k)(1 - f(k))k^2 dk F(k) \qquad (3)$$

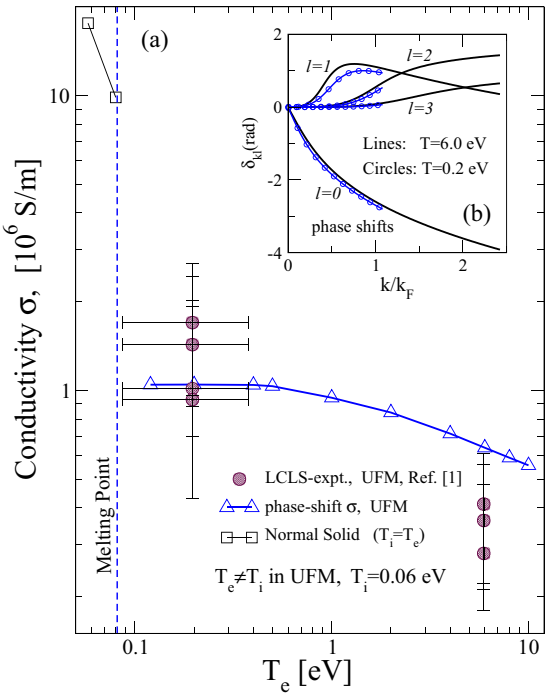

FIG. 2. (a) The static conductivity $\sigma(0)$ of aluminum in the UFM state. LCLS experiment and the $\sigma(0)$ from theory, with $T_i \neq T_e$, for a range of T_e. (b) The low-angular-momentum phase shifts δ_{kl} used for the conductivity calculation are shown at two electron temperatures for $l = 0$–3, as a function of k/k_F.

$$F(k) = \int_0^{2k} q^3 \Sigma(q,k) S(q) dq;\ q = k(1-\cos\theta)^{1/2},$$

$$\Sigma(k,q) = \left| k^{-2} \sum_l (2l+1) e^{i\delta_{kl}} \sin(\delta_{kl}) P_l(\cos\theta) \right|^2. \quad (4)$$

The original numerical implementation (see the Appendix, Ref. [28]) has been improved, using up to 38 l states if needed, an energy cutoff of $E_F + 2T_e$ with asymptotic corrections. Typical δ_{kl} from the NPA are shown in Fig. 2(b). Results for $\sigma(0)$ for isochoric Al, from Eq. (3) covering 0.2 to 10 eV, are given in Fig. 2(a) while $\sigma(0)$ up to 100 eV are in Table 1 of Ref. [29]. The conductivity changes very little as the $S(q)$ and $\Sigma(k,q)$ remain essentially unchanged in the isochoric material where T_e/E_F changes only from ∼0.002 to ∼0.51. Changes in the conductivity are due to the change in the smearing of the Fermi surface [Fig. 1(b)] via the $f(k)\{1-f(k)\}$ thermal factor. The differences in the transport properties of UFM aluminum and normal equilibrium aluminum in the WDM state are highlighted in Fig. 3, where static conductivity calculations are presented. The conductivity of normal liquid aluminum (2.7 g/cm^3) with $T_i = T_e$ for the 0.1 eV $\leqslant T_e \leqslant$ 10 eV reported by Sjostrom *et al.* [27] is seen to be about a factor of 2 to 5 higher than the conductivity of UFM aluminum, calculated using phase shifts or in comparison with the two experimental data points [1]. The weak-scattering approximation to the conductivity uses the Ziman formula which invokes the pseudopotential $W(q)$ and the ion structure factor $S(q)$ calculated from it at $T_i = 0.06$ eV, depicted in Fig. 1. The

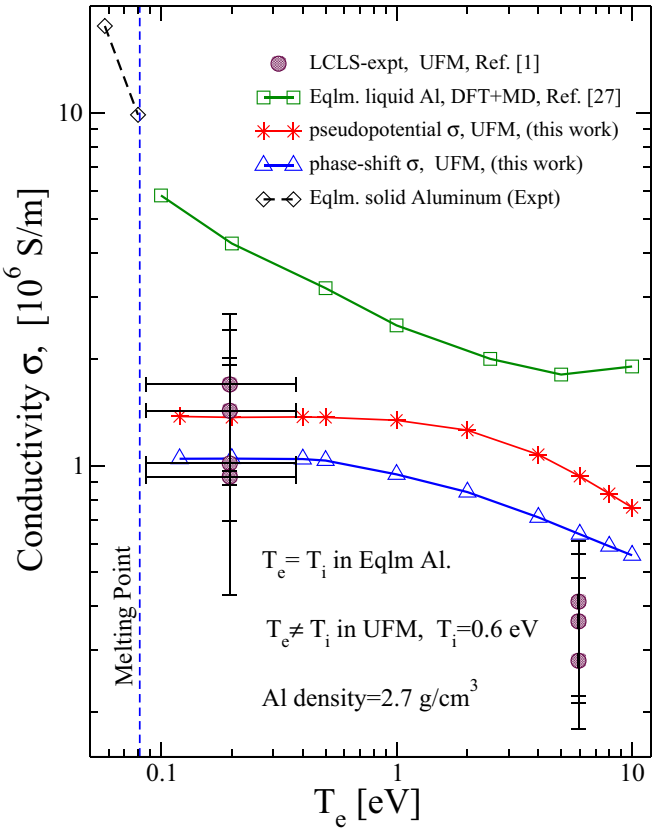

FIG. 3. The static conductivity $\sigma(0)$ of normal liquid aluminum from MD+DFT is compared with that of UFM aluminum. Some data for the normal solid are also shown. The DFT+MD ($T_i = T_e$) calculation (boxes) (Ref. [27]) assumes that $T_e = T_i$, i.e., normal molten aluminum. A weak-scattering approximation calculation (using the NPA pseudopotential) and a strong-scattering calculation (from the NPA phase shifts, see Fig. 2) for UFM-Al with the ions "frozen" at $T_i = 0.06$ eV are presented.

strong-scattering calculation using phase shifts to calculate the conductivity is shown as triangles. Both the strong-scattering calculation and the weak-scattering calculation approximate the two available UFM data points better than the equilibrium DFT+MD simulation. This supports the picture where the WDM aluminum in the experiment is better modeled as a $2T$ UFM system. It should be noted that a DFT+MD calculation of the UFM aluminum conductivity, with the aluminum ions frozen at $T_i = 0.06$ eV, cannot be conveniently achieved using available simulation methods because generating enough ionic configurations for a solid at $T_i = 0.06$ eV to dampen the random oscillations in the calculated $\sigma(\omega)$ is beyond our reach. Hence the NPA phase-shifts approach seems to be practically the only method currently available for including strong electron-ion collision effects in a reliable way.

The above physical picture can be exploited to construct a simple revalidation of the Ziman formula as well as the dynamic relaxation-frequency formula. We refit the pseudopotential so that the Ziman formula reproduces the strong-scattering static conductivity $\sigma(0)$ obtained from the phase shifts. An Ashcroft pseudopotential $V_A(r_c)$ specified only by the core radius r_c could be found to reproduce the $\sigma(0)$ obtained

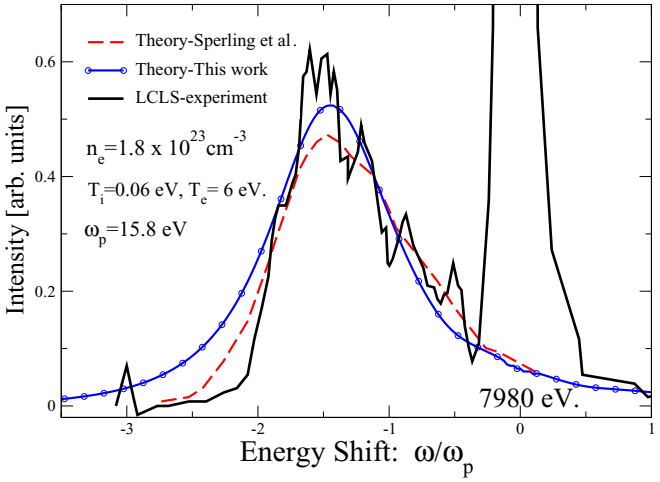

FIG. 4. The UFM-aluminum plasmon line shape at $T_e = 6$ eV, from experiment and theory.

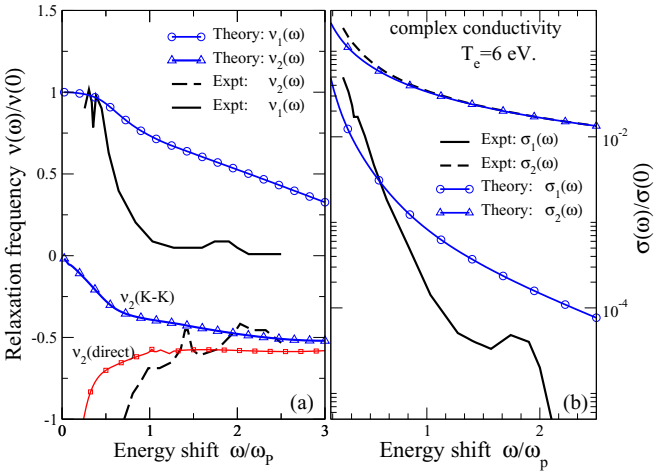

FIG. 5. (a) Theory and experiment for the momentum-relaxation frequency ν_1 and ν_2 versus the energy shift ω/ω_p. $\nu_2(\omega)$ calculated from $\nu_1(\omega)$ via Kramers-Krönig and via a direct numerical procedure are shown. (b) $\sigma_1(\omega)$ and $|\sigma_2(\omega)|$ from experiment and theory.

from the phase-shift calculation in the range $T_e = 0.2$ to 6 eV. This r_c is consistent with the NPA value of the bound core of the Al^{3+}. We use this pseudopotential $V_A(r_c)$ instead of $W(q)$ in Eq. (1) to evaluate $\nu_1(\omega) + i\,\nu_2(\omega)$.

IV. THE PLASMON PROFILE AND $\nu(\omega)$

An important result of the LCLS experiment is the plasmon profile from UFM aluminum. We discuss $T = 6$ eV in detail. Equation (1) evaluates $\nu_1(\omega)$ and $\nu_2(\omega)$ using the $V_A(r_c)$ pseudopotential. Obtaining ν_1 via $\mathrm{Im}\{\chi(q,\omega)\}$ in Eq. (2) and ν_2 via Kramers-Krönig is computationally accurate. A direct estimate of ν_2 is also available from Eqs. (1) and (2). The response function $\chi(q,\omega)$ uses an LFC derived from the finite-T xc potential [16]. The transverse dielectric function $\varepsilon(q \to 0, \omega + i\,\nu(\omega))$ provides the optical scattering cross section $S_{ee}(q \to 0, \omega)$. This is $\propto \mathrm{Im}\{1/\varepsilon(\omega - \nu_2 + i\,\nu_1)\} n_B(\omega)$, where $n_B(\omega)$ is a Bose factor at the electron temperature T_e. Instead of Mermin theory, we use the simplest transverse dielectric function in the $q \to 0$ limit. The calculated scattered intensity is shown in Fig. 4. The predicted profile differs on the red wing of the experimental plasmon line shape. This can arise from shortcomings in theoretical as well as experimental inputs. A $2T$ model may be too simplistic [13], or the refitting using the Ashcroft pseudopotential may be inadequate and a better theory of $\nu(\omega)$ may be needed.

The quantities $\nu(\omega)$ and $\sigma(\omega)$ can be extracted from the experimental $S(q \to 0, \omega)$. We use the $\nu_1(\omega), \nu_2(\omega)$ reported by Sperling *et al.* to test our results, although they assumed a Mermin form to extract the data. That is, we assume that the modeling differences fall within the error bars. The closeness of the plasmon profile of Sperling *et al.* and ours justifies this assumption. In effect, the error of using the Mermin model is partly compensated via the error of using the "improved" Born approximation of Ref. [1], made up of a mixture of many-body theories.

The experimental ν_1^{ex} and ν_2^{ex} are compared with our calculated ν_1, ν_2 in Fig. 5, where the energy shift ω is $\omega_1 - \omega_0$ with $\omega_0 = 7980$ eV and hence negative (for the plasmon studied here). The theoretical ν_1 decays very slowly compared the ν_1^{ex}.

The Drude formula provides $\sigma(\omega)$ from $\nu(\omega)$. Setting $\varpi = \omega - \nu_2$, $d(\omega) = \nu_1(\omega)^2 + \varpi^2$ we use $\alpha = \omega_p^2/(4\pi)$, $\sigma_1(\omega) = \alpha\nu_1/d(\omega)$, and $\sigma_2(\omega) = \alpha\varpi/d(\omega)$. We have recalculated σ_1, σ_2 from our theoretical ν_1, ν_2 given in Fig. 5(a) and from the experimental ν_1, ν_2 at $T = 6$ eV given in Fig. 3 of the Supplemental Material of Ref. [1]. The resulting $\sigma_1(\omega), \sigma_2(\omega)$ are displayed in Fig. 5(b). Note that although $\sigma_2(\omega)$ is expected to tend to zero as $\omega \to 0$, this happens only quite close to $\omega = 0$ because of the strong negativity seen in both experimental and theoretical numbers for ν_2 [see Fig. 5(a)]. Although σ_1 is close to the experiment for small ω, it deviates from experiment as ω increases.

V. CONCLUSION

In conclusion, we have questioned popular paradigms in modeling warm-dense ultra-fast-matter systems. These are (i) the use of the Mermin response function with its assumptions of rapid local thermodynamic equilibrium and (ii) the use of ion distributions with relative laxity (e.g., even hard-sphere distributions), with $T_e = T_i$ even for ultrafast matter. (iii) The use of a mixture of theoretical models with little regard to consistency is contrasted with the DFT-NPA model where all the needed quantities are calculated from the output of a Kohn-Sham equation. As the DFT-NPA is an effectively "single-ion" and "single-electron" Kohn-Sham calculation in the sense of DFT, it is orders of magnitude faster than the many-center "single-electron" DFT approach used in large solid-state electronic codes. Furthermore, the method uses the modified hyper-netted-chain equation instead of molecular dynamics to generate the structure factors that are needed in the theory. The static and dynamic conductivity, structures factors, and plasmon profiles, calculated for $2T$ ultrafast aluminum within DFT-NPA, give good agreement with the LCLS data. (iv) The static conductivity of ultrafast matter

is shown to be significantly lower than that of equilibrium WDM aluminum. (v) Validity (or not) of the simple Born approximation to the dynamic conductivity is examined. We show that the Born approximation using a pseudopotential fitted to the strong-scattering conductivity $\sigma(0)$ obtained via phase shifts successfully predicts the plasmon line shape and the dynamic conductivity of the LCLS experiment, without invoking the Mermin model and thermodynamic equilibrium.

ACKNOWLEDGMENTS

The author thanks Heide Reinholz, Philipp Sperling, and colleagues for their comments.

[1] P. Sperling, E. J. Gamboa, H. J. Lee, H. K. Chung, E. Galtier, Y. Omarbakiyeva, H. Reinholz, G. Röpke, U. Zastrau, J. Hastings, L. B. Fletcher, and S. H. Glenzer, Phys. Rev. Lett. **115**, 115001 (2015).

[2] S. Glenzer and R. Redmer, Rev. Mod. Phys. **81**, 1625 (2009).

[3] Andrew Ng, Int. J. Quant. Chem. **112**, 150 (2012).

[4] J. Clérouin, Grégory Robert, Philippe Arnault, Christopher Ticknor, Joel D. Kress, and Lee A. Collins, Phys. Rev. E **91**, 011101 (2015).

[5] Jie Chena, Wei-Kan Chenb, Jau Tangc, and Peter M. Rentzepisb, Proc. Natl. Acad. Sci. USA **108**, 18887 (2011).

[6] H. M. Milchberg, R. R. Freeman, S. C. Davey, and R. M. More, Phys. Rev. Lett. **61**, 2364 (1988).

[7] M. W. C. Dharma-wardana, Solid State Commun. **86**, 83 (1993).

[8] F. R. Graziani *et al.*, Lawrence Livermore Nat. Lab. Report No. LLNL-JRNL-469771 (2011).

[9] F. Perrot, Phys. Rev. E **47**, 570 (1993).

[10] F. Perrot and M. W. C. Dharma-wardana, Phys. Rev. E **52**, 5352 (1995).

[11] M. W. C. Dharma-wardana, Contrib. Plasma Phys. **55**, 85 (2015).

[12] M. W. C. Dharma-wardana and F. Perrot, Phys. Lett. A **163**, 223 (1992).

[13] N. Medvedev, U. Zastrau, E. Förster, D. O. Gericke, and B. Rethfeld, Phys. Rev. Lett. **107**, 165003 (2011); D. A. Chapman and D. O. Gericke, *ibid.* **107**, 165004 (2011); Alberto G. de la Varga *et al.*, High Energy Density Phys. **9**, 542 (2013).

[14] B. Wilson, V. Sonnad, P. Sterne, and W. Isaacs, J. Quant. Spectrosc. Radiat. Transf. **99**, 658 (2006).

[15] D. D. Burrill, D. V. Feinblum, M. R. J. Charest, and C. E. Starrett, High Energy Density Phys. **19**, 1 (2016).

[16] F. Perrot and M. W. C. Dharma-wardana, Phys. Rev. B **62**, 16536 (2000); **67**, 079901(E) (2003).

[17] M. W. C. Dharma-wardana, arXiv:1602.04734v1.

[18] L. Harbour, M. W. C. Dharma-wardana, D. D. Klug, and L. Lewis, Contrib. Plasma Phys. **55**, 144 (2015).

[19] V. Recoules, J. Clérouin, G. Zérah, P. M. Anglade, and S. Mazevet, Phys. Rev. Lett. **96**, 055503 (2006).

[20] M. W. C. Dharma-wardana and G. C. Aers, Phys. Rev. B **28**, 1701 (1983).

[21] Hopfield, Phys. Rev. **139**, A419 (1965).

[22] N. D. Mermin, Phys. Rev. B **1**, 2362 (1970).

[23] H. Reinholz, R. Redmer, G. Röpke, and A. Wierling, Phys. Rev. E **62**, 5648 (2000).

[24] M. W. C. Dharma-wardana, Phys. Rev. E **64**, 035401 (2001).

[25] G. F. Giuliani *et al.*, *Quantum Theory of the Electron Liquid* (Cambridge University Press, Cambridge, 2005), Sec. 4.6.

[26] G. D. Mahan, *Many Particle Physics* (Plenum, New York, 1981), Sec. 8.1.

[27] T. Sjostrom and Jérôme Daligault, Phys. Rev E **92**, 063304 (2015).

[28] F. Perrot and M. W. C. Dharma-wardana, Phys. Rev. A **36**, 238 (1987).

[29] F. Perrot and M. W. C. Dharma-wardana, Int. J. Thermophys. **20**, 1299 (1999).